

# Intra-Day DNI Forecasting Under Clear Sky Conditions Using ANFIS

Rémi Chauvin\* Julien Nou\* Stéphane Thil\*<sup>\*,\*\*</sup>  
Stéphane Grieu\*<sup>\*,\*\*</sup>

\* PROMES-CNRS (UPR 8521),  
Tecnosud, Rambla de la thermodynamique, 66100 Perpignan, France

\*\* University of Perpignan Via Domitia,  
52 Avenue Paul Alduy, 66860 Perpignan, France

Tel.: +334-6868-2222; e-mail: [firstname.lastname@promes.cnrs.fr](mailto:firstname.lastname@promes.cnrs.fr)

---

**Abstract:** The present paper deals with the development of a new intra-day Direct Normal Irradiance (DNI) forecasting methodology, under clear sky conditions. Indeed, one challenge of the CSPIMP (Concentrated Solar Power plant efficiency IMProvement) research project is to forecast the sun's resource accurately and design efficient plant control approaches. First, a quick review of the different formulations available for the atmospheric turbidity coefficient (from which DNI can be calculated) is performed. The data selection and filtering process is then described. Finally, the new forecasting approaches are compared to persistent and autoregressive models. The most efficient model presented here is based on side-by-side Adaptive Network-based Fuzzy Inference Systems (ANFIS). The selected configuration achieves very good results and validates the proposed forecasting methodology.

*Keywords:* direct normal irradiance, atmospheric turbidity, clear sky conditions, forecasting techniques, adaptive network-based fuzzy inference system.

---

## 1. INTRODUCTION

In a context of sustainable development, clean energy systems are strongly promoted in the European energy mix. Among the various solar energy systems, the Concentrating Solar Power (CSP) systems will play a key role in the future. At this stage, the main drawback of this technology continues to be its cost. To overcome it, the European research project CSPIMP (Concentrated Solar Power plant efficiency IMProvement) has been recently initiated. Its main target is to achieve a better competitiveness of the CSP plants thanks to the development of new tools improving steam turbine start up cycles, maintenance activities and plant control.

One challenge of the project is to forecast the sun's resource accurately. Indeed, it is widely acknowledged by producers and grid operators that solar energy variability strongly influences the CSP systems output. Therefore, Direct Normal Irradiance (DNI) forecasting would help them to efficiently schedule and manage the electricity production according to the grid needs. Different forecasting methodologies have already been proposed for various time horizons [Diagne et al. 2013]. Changes in DNI are mainly related to clouds motion, which can be detected using sky or satellite imagery [Mefti et al. 2008] [Chow et al. 2011] [Marquez and Coimbra 2013] [Cazorla et al. 2008]. However, when there is no clouds, the atmospheric turbidity, mainly attributable to the Aerosol Optical Depth (AOD), is known to be the driving factor [Gueymard 2012b]. As a consequence, it has been decided to split the DNI forecasting process into two different blocks: cloud

cover forecasting and DNI forecasting under clear sky conditions. In this paper, only clear sky DNI forecasting at different short-time horizons is studied.

First, a quick review of the different formulations available for the atmospheric turbidity coefficient is introduced (section 2). The next section (section 3) briefly describes the database used to develop and validate our forecasting models as well as the multi-resolution analysis performed to extract the clear sky data. Section 4 deals with these models, especially the neuro-fuzzy approaches (side-by-side and single-block ANFIS). With the exception of persistent model 1, DNI is calculated from the forecasted values of atmospheric turbidity at short term horizon (up to 5 hours). In section 5, the forecasting performances are compared and discussed. The paper ends with a conclusion and outlook on further work (section 6).

## 2. CONSIDERATIONS ABOUT ATMOSPHERIC TURBIDITY

Under clear sky conditions, the broadband DNI ( $I_{CS}$ ) is:

$$I_{CS} = r \cdot I_0 \cdot T \quad (1)$$

where  $I_0$  is the solar constant ( $I_0 = 1367 \text{ W/m}^2$ ),  $r$  is the sun-earth distance correction factor and  $T$  the atmospheric transmittance resulting from both scattering and absorption of the sunlight.  $r$  is assumed to be constant through the day. The knowledge of the clear sky atmospheric transmittance is thus required to assess the amount of direct solar energy reaching the ground. This attenuation factor  $T$  is correlated to the band transmittances of Rayleigh scattering ( $T_{Ra}$ ), uniformly mixed gases

absorption ( $T_g$ ), ozone absorption ( $T_{O_3}$ ), nitrogen dioxide absorption ( $T_{NO_2}$ ), water vapor absorption ( $T_w$ ) and aerosol absorption ( $T_{AOD}$ ) as follows [Gueymard 2008]:

$$T = T_{Ra} \cdot T_g \cdot T_{O_3} \cdot T_{NO_2} \cdot T_w \cdot T_{AOD} \quad (2)$$

Information regarding these atmospheric attenuation coefficients can be obtained using radiation transfer models based on site pressure, ozone amount, total nitrogen dioxide amount, precipitable water and Ångström turbidity coefficients as input parameters. These transmittances are also function of the sunlight optical path length ( $m$ ) through the atmosphere, also called air mass. Among all clear-sky broadband radiation transfer models of the literature, REST2 [Gueymard 2008] has proven to forecast DNI with unsurpassed accuracy [Gueymard and Myers 2008] [Gueymard 2012a]. However, the model requires AOD data which happens to be difficult to measure, as well as rarely available [Gueymard 2012b]. As a consequence, radiation transfer models are not well adapted for on-site real-time clear sky DNI forecasting. On the other hand, simpler models, based on a broadband turbidity coefficient like the well-known Linke turbidity coefficient ( $T_{LK}$ ) [Linke 1922], have been developed. Although they have a lower accuracy than radiation transfer models, they have been widely used by the scientific community because they only derive from broadband beam radiation measurement networks and can thus be easily implemented.

The Linke turbidity coefficient ( $T_{LK}$ ) represents the number of clean dry atmospheres leading to the observed attenuation of solar radiation. The average Linke turbidity is close to 3 in most parts of Europe whereas it can grow up to 6 or 7 in highly polluted cities. Although this coefficient is easy to calculate, one of its main drawbacks remains its strong dependency on air mass [Kasten 1988] [Grenier et al. 1994] [Kasten and Young 1989]. That is why, in 2002, Ineichen and Perez proposed a new formulation of the Linke turbidity coefficient ( $T_{LI}$ ) in order to limit this turbidity dependence upon solar geometry [Ineichen and Perez 2002]. They obtained a new empirical formulation of the broadband atmospheric transmittance for the normal beam clear sky radiation (3):

$$T = f(m, T_{LI}) = b \cdot \exp[-0.09 \cdot m(T_{LI} - 1)] \quad (3)$$

This equation matches with the Linke turbidity coefficient at air mass 2 ( $f(2, T_{LK}) = f(2, T_{LI})$ ) and includes the effects of both scattering and absorption phenomena. It is also corrected by a multiplicative coefficient  $b$  taking into account the altitude ( $alt$ ) of the considered site:

$$b = 0.664 + \frac{0.163}{\exp(-alt/8000)} \quad (4)$$

From (1) and (3), Ineichen has obtained a new formulation for the turbidity coefficient with much better stability than the previous one:

$$T_{LI}(t) = 1 + \left[ \frac{11.1}{m(t)} \cdot \ln \left( \frac{b \cdot r \cdot I_0}{I_{CS}(t)} \right) \right] \quad (5)$$

Because this coefficient can be easily derived from broadband beam radiation measurements, it has been selected as a starting point for the development of our intra-day clear sky DNI forecasting models.

### 3. DATA PRE-PROCESSING

The database used to develop and validate the different forecasting models is derived from data collected at the National Renewable Energy Laboratory, located in Golden, Colorado, USA. Data are freely available at <http://midcdmz.nrel.gov/apps>, where an exhaustive set of meteorological parameters and irradiances are collected and stored since July 1981. In our study, only data ranging from 2002 to 2013 have been considered.

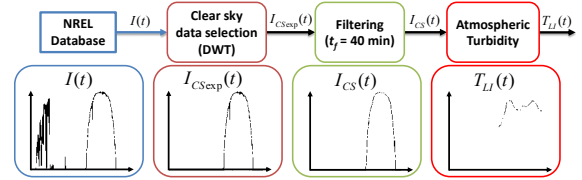


Fig. 1. Data pre-processing methodology.

According to (5), the following data have been collected: timestamp, air mass ( $m$ ), extraterrestrial irradiance ( $I_0$ ) and direct normal irradiance ( $I$ ). However, the irradiances collected have been measured for clear sky and cloudy sky conditions, whereas our models have to be developed only for clear sky days. As a consequence, a filtering method based on a DWT (Discrete Wavelet Transform) multi-resolution analysis has been used in order to treat the DNI signal and extract the days of interest (Fig. 1). Using a bank of filters composed of Low-Pass (LP) and High-Pass (HP) filters, the DNI signal ( $I$ ) is decomposed into approximation and detail coefficients. The process can be repeated  $n$  times, and produces  $n$  levels of decomposition. Different families of wavelets may be chosen for analyzing sequences of data points. Because the Daubechies wavelets [Daubechies 1992] have the highest number of vanishing moments, this family has been chosen. The impact on performance of both the decomposition level and the wavelet order has also been studied: a decomposition of level 3 using 4th-order Daubechies wavelets has been shown to be optimal [Nou et al. 2013]. Clear sky data were selected by thresholding the detail of level 3 and removing the low values of  $I$  from the database. The clear sky irradiance threshold has been set to  $150 \text{ W/m}^2$  because such a value refers to the typical minimum solar irradiance usable in CSP plants. With this selection, only full clear sky days were selected. Indeed, full days allow keeping the transient behavior of the turbidity, which is essential in order to develop our forecasting models. A temporal smoothing, using a moving average of 40 minutes, is then applied downstream on these selected days in order to remove the last outliers. From these selected days, turbidity is computed using (5). The final database specifications are reported in Table 1.

Table 1. Database specifications.

Description	Value
Latitude	39.74 N
Longitude	105.18 W
Altitude	1829 m
Number of selected clear sky days	156
Distribution [Spring Summer Autumn Winter]	[22 45 53 36]
Yearly mean turbidity	2.37

#### 4. MODELS

Different models have been developed and compared for forecast horizons varying from 30 minutes to 5 hours (Fig. 2). These forecast horizons ( $\Delta t$ ) have been chosen because they typically represent the window needed by the operators of a plant to schedule an intra-day management strategy (storage system, backup generator...) efficiently. The first category of models (in blue on Fig. 2) is based on daily, monthly and yearly mean turbidity values. This approach allows the gain of accuracy obtained from a yearly atmospheric turbidity coefficient to a daily one to be evaluated. The second category (in pink on Fig. 2) consists in two simple persistent models and an autoregressive one. These models are used as reference models. The last category (in orange on Fig. 2) is based on neuro-fuzzy techniques (i.e. ANFIS).

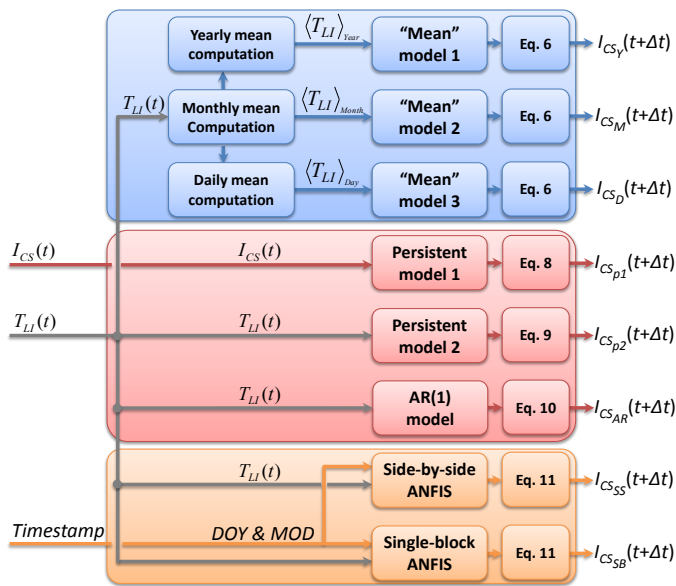


Fig. 2. Overview of the developed models.

##### 4.1 Mean turbidity-based models

It is known that atmospheric turbidity has seasonal trends. Turbidity is higher in summer than it is in winter, because of a higher concentration in aerosol. So, we decided first for models based on yearly, monthly or daily mean turbidity values. Fig. 3 summarizes the mean values of turbidity through the year using the collected database. As expected, a seasonal trend of the turbidity can be observed with a peak during summer time. The yearly mean turbidity is averaged from the monthly mean turbidity whereas the daily mean turbidity comes from a linear interpolation of the monthly mean turbidity. According to (1) and (3), the expected clear sky irradiance of the collected days can be calculated as follows, with  $k = \{\text{Year, Month, Day}\}$  (6):

$$I_{CS_k}(t + \Delta t) = r \cdot I_0 \cdot f(m(t + \Delta t), \langle T_{LI} \rangle_k) \quad (6)$$

##### 4.2 Persistent and autoregressive models

Two persistent and one autoregressive models have been also developed using the database. The first persistent model considers the DNI as constant between the present

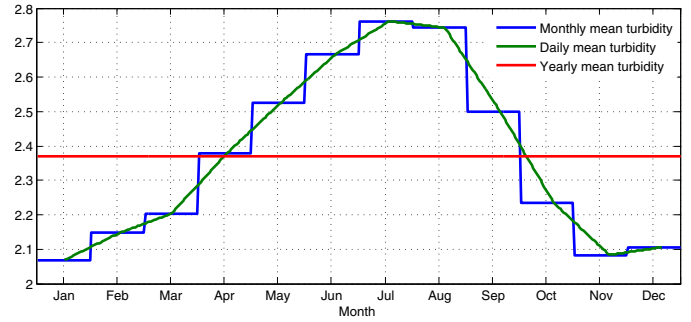


Fig. 3. Yearly, monthly and daily mean turbidity values.

time and the forecast horizon whereas the second one considers the turbidity as constant during the same time interval. Although the first persistent model is not expected to give good results, we considered it in order to highlight the use of the turbidity coefficient as relevant. Regarding the autoregressive model, it has been decided to use a first order equation ( $AR(1)$ ), with  $t = 0, \pm 1, \pm 2, \dots$ , which represents a standard linear difference:

$$T_{LI}(t + 1) = AR(T_{LI}(t)) = \rho \cdot T_{LI}(t) + \epsilon_t \quad (7)$$

We minimized the least-squares criterion in order to determine the parameters of (7). From these 3 models, irradiance can be expressed as follows:

$$I_{CS_{p1}}(t + \Delta t) = I_{CS}(t) \quad (8)$$

$$I_{CS_{p2}}(t + \Delta t) = r \cdot I_0 \cdot f(m(t + \Delta t), T_{LI}(t)) \quad (9)$$

$$I_{CS_{AR}}(t + \Delta t) = r \cdot I_0 \cdot f(m(t + \Delta t), T_{LI}(t + \Delta t)) \quad (10)$$

##### 4.3 ANFIS models

The new forecasting models presented in this paper are based on a well known neuro-fuzzy technique. Because ANFIS is a powerful architecture, it has been chosen to forecast the clear sky DNI. In the field of artificial intelligence, feedforward neural networks and fuzzy logic can be combined in order to synergize the two techniques by adding together the human-like reasoning style of fuzzy systems (through the use of a linguistic model consisting in a set of if-then fuzzy rules) with the learning ability and connectionist structure of artificial neural networks [Lin and Lee 1996, Abraham 2005]. An ANFIS is a 5-layer architecture based on the Takagi-Sugeno fuzzy inference system. Such an architecture can be used to interpret an input/output map after a training phase. First, a parameterized structure is hypothesized and, using an iterative and hybrid optimization method (basically, a combination of least squares estimation and backpropagation gradient descent method), the membership function parameters are adjusted, the consequent parameters are identified and a rule base is designed. The training process stops whenever the maximum number of iterations is reached or the training error goal is achieved.

The first forecasting approach (Fig. 4.a) is composed of ten ANFIS blocks. Each block deals with forecasting atmospheric turbidity at a specific horizon ranging between 30 minutes and 5 hours. The Day Of the Year (*DOY*), the Minute Of the Day (*MOD*) and the atmospheric turbidity at time  $t$  ( $T_{LI}(t)$ ) are the blocks inputs. The second approach (Fig. 4.b) consists in a single recurrent

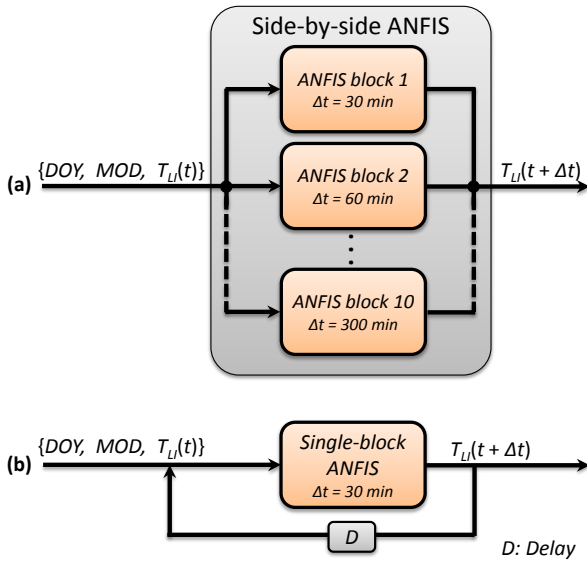


Fig. 4. The two neuro-fuzzy forecasting approaches.

ANFIS block that produces forecasts with a time step of 30 minutes, until the horizon is reached. Inputs remain unchanged. Whatever the ANFIS approach, direct normal irradiance ( $I_{CS_{SS,SB}}(t + \Delta t)$ ) is calculated from the forecasted values of atmospheric turbidity ( $T_{LI}(t + \Delta t)$ ).

$$I_{CS_{SS,SB}}(t + \Delta t) = r \cdot I_0 \cdot f(m(t + \Delta t), T_{LI}(t + \Delta t)) \quad (11)$$

We considered the Mean Absolute Error (MAE) and the Normalized Root-Mean-Square Error (NRMSE) as performance criteria in order to evaluate the eight approaches.

## 5. RESULTS

In this section we present first the constraints on the models regarding clear sky DNI forecasting. Then, the way the side-by-side and single-block ANFIS models are parameterized is described. Finally, we carried out a comparative study of the neuro-fuzzy (i.e. the ANFIS-based) and standard models.

### 5.1 Forecasting issues

The main drawback of the clear sky DNI forecasting remains the discontinuity of data due to nights and cloud events. As previously mentioned, we only selected full clear sky days in order to preserve the transient behavior of atmospheric turbidity through the day. However, such days are rarely one after the other. In addition, whatever the approach, the first atmospheric turbidity value is obtained after sunrise and, as a result, the first clear sky DNI forecast will be available at sunrise plus horizon. For instance, if sunrise occurs at 8:00 AM and the forecast horizon is set to 5 hours, then the first forecasted value will be available at 01:00 PM. This is the main reason why models based on mean values (independent of time) of atmospheric turbidity are so convenient. However, and because of the ability of artificial intelligence tools to forecast time series with good accuracy, we decided to test neuro-fuzzy techniques in order to develop new models and improve performance. If the proposed approaches are conclusive, a real-time strategy will be implemented in order to fill the gap produced by nights and clouds.

### 5.2 ANFIS settings

A parametric study has been performed for both the side-by-side and the single-block ANFIS. The goal is to optimize the structure of the neuro-fuzzy systems used in order to get the best possible accuracy for each forecast horizon. Among the possibilities of optimization, we focused on the number of observations to be considered ( $T_{LI}$ ), the number of fuzzy sets used to split the universes of discourse of the model inputs and the number of training examples.

*Side-by-side ANFIS.* Due to the structure of the model, considering more than one observation is not relevant. Indeed, it has been highlighted above that forecasted values are not available while the horizon is not elapsed. Two observations and a 5-hour forecast horizon would lead to forecasted values available 10 hours after sunrise time, which makes no sense in our case. Nevertheless, the way the universes of discourse are partitioned into fuzzy sets is studied. The side-by-side ANFIS are composed of 3 inputs each and Gaussian membership functions are associated to the sets. Because of computational limitations, only a number of fuzzy sets ranging between 2 and 5 for each block input has been considered. Among the 64 possible fuzzy partitions, only the partitions producing the lowest NRMSE, for a given number of rules, are presented with their confidence interval (Fig. 5). Table 2 lists the selected fuzzy partitions for three forecast horizons varying from 1 to 5 hours. It can be noticed that the optimization through the partitioning process becomes insignificant very quickly. As an example, at  $t + 5$  hours, the difference in accuracy (NRMSE) between configurations [5 4 5] and [5 5 5] is  $0.7 \text{ W/m}^2$  for  $1000 \text{ W/m}^2$  only. So, one can assume that more than 5 sets to split the universes of discourse does not impact accuracy in a significant way (but complexity increases) and we decided for fuzzy configuration [5 5 5].

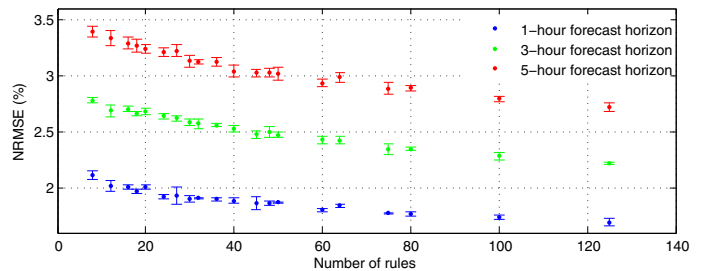


Fig. 5. NRMSE ( $I_{CS}$ ) as a function of the number of fuzzy sets used to split the universes of discourse.

Once the ANFIS partition is defined, one can search for the optimal number of examples to be used during the training phase. Table 3 depicts the NRMSE as a function of the number of training examples, using configuration [5 5 5] and considering forecast horizons of 1, 3 and 5 hours. An increase in the number of training examples from 30000 to 40000 leads to a difference in accuracy less than 0.02 percentage point, whatever the horizon. In addition, too many examples can lead to the design of redundant fuzzy rules as well as over-parameterized models. So, we decided to limit the number of training examples to 40000.

*Single-block ANFIS.* A similar parametric study has been performed for the single-block approach. As previously stated, this approach is based on a recurrent ANFIS

Table 2. Fuzzy partition of DOY, MOD and atmospheric turbidity and NRMSE ( $I_{CS}$ ).

Number of rules	Fuzzy configuration			NRMSE (%)		
	t+1h	t+3h	t+5h	t+1h	t+3h	t+5h
8	[2 2 2]	[2 2 2]	[2 2 2]	2.11	2.78	3.39
12	[2 3 2]	[2 3 2]	[2 2 3]	2.02	2.69	3.33
16	[2 4 2]	[2 2 4]	[4 2 2]	2.01	2.70	3.29
18	[2 3 3]	[3 3 2]	[3 3 2]	1.97	2.66	3.27
20	[2 5 2]	[5 2 2]	[5 2 2]	2.01	2.68	3.24
24	[2 3 4]	[4 3 2]	[4 2 3]	1.92	2.64	3.21
27	[3 3 3]	[3 3 3]	[3 3 3]	1.94	2.62	3.22
30	[2 3 5]	[5 2 3]	[5 2 3]	1.90	2.59	3.13
32	[2 4 4]	[4 2 4]	[4 2 4]	1.91	2.57	3.12
36	[3 4 3]	[4 3 3]	[4 3 3]	1.90	2.56	3.12
40	[2 5 4]	[4 2 5]	[4 2 5]	1.88	2.53	3.04
45	[5 3 3]	[5 3 3]	[5 3 3]	1.86	2.48	3.02
48	[3 4 4]	[4 3 4]	[4 3 4]	1.86	2.50	3.03
50	[2 5 5]	[5 2 5]	[5 2 5]	1.87	2.47	3.02
60	[5 4 3]	[4 3 5]	[5 4 3]	1.80	2.43	2.94
64	[4 4 4]	[4 4 4]	[4 4 4]	1.84	2.43	2.99
75	[5 5 3]	[5 3 5]	[5 3 5]	1.77	2.35	2.89
80	[5 4 4]	[5 4 4]	[5 4 4]	1.77	2.35	2.89
100	[5 4 5]	[5 5 4]	[5 4 5]	1.74	2.28	2.79
125	[5 5 5]	[5 5 5]	[5 5 5]	1.69	2.22	2.72

Table 3. NRMSE (%), ( $I_{CS}$ ) as a function of the training examples (side-by-side ANFIS).

Examples	t+1h	t+3h	t+5h
20000	1.86	2.29	2.76
30000	1.69	2.24	2.73
40000	1.69	2.22	2.72

block. Due to its structure, evaluating the impact of the number of observations on the final result is now possible. Indeed, the output of the single-block ANFIS is recursively used, with a time step of 30 minutes, until the desired forecasting horizon is reached. Using such a structure, forecasts are available only 30 minutes after sunrise for every forecasting horizon. However, as previously highlighted, the constraints on our database (i.e. discontinuities) as well as some divergence effects limit the number of observations usable as model inputs. So, we considered up to three previous values. The results are reported in Table 4.

Table 4. NRMSE (%), ( $I_{CS}$ ) as a function of the number of observations and training examples (single-block ANFIS).

Examp.	t+1h			t+3h			t+5h		
	[1]	[2]	[3]	[1]	[2]	[3]	[1]	[2]	[3]
10000	2.12	1.98	2.29	3.04	3.12	X	3.76	3.94	X
20000	2.12	1.95	2.33	3.08	3.02	X	3.79	3.90	X
30000	2.13	1.96	1.93	3.02	3.04	X	3.78	3.94	X
40000	2.10	1.95	1.95	3.05	3.00	X	3.74	3.84	X

X is for divergence and [n] is for the number of observations

From this table, it can be noticed that an increase in the number of observations does not improve accuracy in a significant way. For a forecast horizon set to 1 hour, accuracy is slightly improved when considering 2 observations ( $T_{LI}(t)$  and  $T_{LI}(t - 30 \text{ min})$ ). However, it is not the case at longer forecast horizon. The model even shows some instability beyond 3 hours, using 3 observations. As a result, we decided to keep only one observation and

10000 examples. Regarding the partition of the universes of discourse, we performed in the same way than for the side-by-side ANFIS parametrization. In this case, the fuzzy configuration does not really impact on accuracy and we finally decided for configuration [2 2 2] in order to limit the complexity of the model (the number of fuzzy rules is reduced) and improve its stability, whatever the forecasting horizon. Table 5 summarizes the characteristics of both the side-by-side and the single-block ANFIS.

Table 5. Characteristics of the ANFIS models.

Characteristics	Side-by-side	Single-block
Membership functions type	“gbell”	“gbell”
Number of training examples	40000	10000
Fuzzy partition	[5 5 5]	[2 2 2]
Number of parameters	545	50
Number of fuzzy rules	125	8

### 5.3 Forecasting results and discussion

In this section, we compare the results given by the neuro-fuzzy approaches and those produced by the basic models (categories 1 and 2). Fig. 6 and 7 summarize these results. The persistent model only based on irradiance (persistent model 1) is not considered here because error is too high to be displayed: NRMSE = 31% at  $t + 5$  hours ( $I_{CS}$ ). Due to very similar results, the light-blue curve is about the NRMSE obtained with both the autoregressive model of order 1 and the persistent model 2 (Fig. 6 and 7).

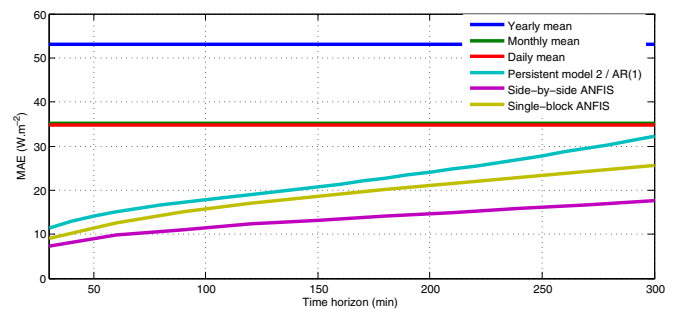


Fig. 6. MAE ( $I_{CS}$ ) as a function of the forecast horizon.

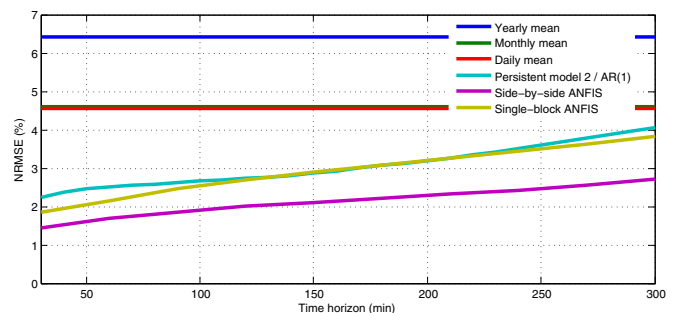


Fig. 7. NRMSE ( $I_{CS}$ ) as a function of the forecast horizon.

As expected, the benefits in considering atmospheric turbidity is obvious: accuracy is increased of about 30% for a 5-hour forecast horizon. One can highlight the stability of the turbidity coefficient in comparison to the variability of sun irradiance through the day. Regarding the models based on mean values of turbidity, both the MAE and

NRMSE are unchanged over the forecasting horizon. In addition, forecasts based on monthly mean values of turbidity outperform forecasts based on yearly mean values (the difference in NRMSE is 1.8 points). This is due to the seasonal trend depicted earlier in the paper. Forecasts based on daily mean values of turbidity do not much better than forecasts based on monthly mean values (difference is negligible) and, as a result, there is no real benefits in interpolating turbidity below the month scale. In other words, the intra-month variability of turbidity is more influenced by the day-by-day atmospheric phenomena than by the overall evolution of the atmosphere through the year. Finally, both the AR(1) model and the persistent model 2 outperform the models based on mean turbidity values even if at  $t+5$  hours the MAE and NRMSE are very close (difference is 0.5 point). Whatever the error criterion (MAE or NRMSE), the side-by-side ANFIS clearly gives the best forecasting results. The single-block ANFIS is almost equivalent to the persistent model 2 if we consider the NRMSE only: 3.76 % (single-block ANFIS) vs. 4.05 % (persistent model 2) at  $t+5$  hours. However, it gives better results than the persistent model 2, on the basis of the MAE:  $26 \text{ W/m}^2$  (single-block ANFIS) vs.  $32 \text{ W/m}^2$  (persistent model 2), again at  $t+5$  hours. It means that the single-block ANFIS produces clear sky DNI forecasting with a higher accuracy than the persistent model 2 (MAE is lower) but with more outlier values than the side-by-side ANFIS (NRMSE is higher). So, among the eight modelling approaches we tested, the side-by-side ANFIS model appears to forecast clear sky DNI with unsurpassed accuracy (NRMSE = 2.72 % at  $t+5$  hours).

## 6. CONCLUSION

The error calculated between the measured DNI and the expected ones, using a daily mean value of atmospheric turbidity ( $\text{NRMSE}_{(Day)} = 4.6 \%$ ), encouraged us to develop intra-day forecasting models of the clear sky irradiance. As a consequence, two different approaches based on Adaptive Network-based Fuzzy Inference Systems (ANFIS) have been developed in order to forecast clear sky DNI for a time horizon varying from 30 minutes to 5 hours. Both approaches outperformed the persistent models and the side-by-side ANFIS provided the best results. However, this model is not easy to implement because of its structure. As a result, a single recurrent ANFIS block that gives forecasts with a time step of 30 minutes, until the fixed horizon is reached, has also been developed. It has the huge advantage to be less complex, easier to optimize and more easily adaptable to different time scales. Nevertheless, it produces slightly less accurate forecasts than the side-by-side ANFIS. Finally, designing DNI neuro-fuzzy forecasting models for a solar power plant like Andasol 1 (180 GWh/year) would increase the forecast accuracy of the energy involved of about 2 GWh/year and the expected energy benefits could potentially reach several hundreds of MWh/year.

## REFERENCES

Abraham, A. (2005). Adaptation of fuzzy inference system using neural learning. In N. Nedjah and L. de Mourrelle (eds.), *Fuzzy system engineering*, volume 181 of *Studies in Fuzziness and Soft Computing*, 53–83. Springer Berlin Heidelberg.

Cazorla, A., Olmo, F., and Alados-Arboledas, L. (2008). Development of a sky imager for cloud cover assessment. *Journal of the Optical Society of America A*, 25(1), 29–39.

Chow, C.W., Urquhart, B., Lave, M., Dominguez, A., Kleissl, J., Shields, J., and Washom, B. (2011). Intra-hour forecasting with a total sky imager at the UC san diego solar energy testbed. *Solar Energy*, 85(11), 2881–2893.

Daubechies, I. (1992). *Ten lectures on wavelets*, volume 61 of *CBMS-NSF Regional Conference Series in Applied Mathematics*. Society for Industrial and Applied Mathematics.

Diagne, M., David, M., Lauret, P., Boland, J., and Schmutz, N. (2013). Review of solar irradiance forecasting methods and a proposition for small-scale insular grids. *Renewable and Sustainable Energy Reviews*, 27, 65–76.

Grenier, J., De La Casinière, A., and Cabot, T. (1994). A spectral model of Linke's turbidity factor and its experimental implications. *Solar Energy*, 52(4), 303–313.

Gueymard, C.A. (2008). REST2: High-performance solar radiation model for cloudless-sky irradiance, illuminance, and photosynthetically active radiation – validation with a benchmark dataset. *Solar Energy*, 82(3), 272–285.

Gueymard, C.A. (2012a). Clear-sky irradiance predictions for solar resource mapping and large-scale applications: Improved validation methodology and detailed performance analysis of 18 broadband radiative models. *Solar Energy*, 86(8), 2145–2169.

Gueymard, C.A. (2012b). Temporal variability in direct and global irradiance at various time scales as affected by aerosols. *Solar Energy*, 86, 3544–3553.

Gueymard, C.A. and Myers, D.R. (2008). Validation and ranking methodologies for solar radiation models. In V. Badescu (ed.), *Modeling Solar Radiation at the Earth's Surface*, 479–510. Springer Berlin Heidelberg.

Ineichen, P. and Perez, R. (2002). A new air mass independent formulation for the linke turbidity coefficient. *Solar Energy*, 73(3), 151–157.

Kasten, F. (1988). Elimination of the virtual diurnal variation of the Linke turbidity factor. *Meteorologische Rundschau*, 41(3), 93–94.

Kasten, F. and Young, A.T. (1989). Revised optical air mass tables and approximation formula. *Applied Optics*, 28(22), 4735–4738.

Lin, C.T. and Lee, C.G. (1996). *Neural Fuzzy Systems: A Neuro-Fuzzy Synergism to Intelligent Systems*. Prentice-Hall, Upper Saddle River, NJ.

Linke, F. (1922). Transmissions-koeffizient und trübungs-faktor. *Beiträge zur Physik der Atmosphäre*, 10, 91–103.

Marquez, R. and Coimbra, C.F. (2013). Intra-hour DNI forecasting based on cloud tracking image analysis. *Solar Energy*, 91, 327–336.

Mefti, A., Adane, A., and Bouroubi, M. (2008). Satellite approach based on cloud cover classification: Estimation of hourly global solar radiation from meteosat images. *Energy Conversion and Management*, 49, 652–659.

Nou, J., Chauvin, R., Traoré, A., Thil, S., and Grieu, S. (2013). Atmospheric turbidity forecasting using side-by-side ANFIS. In *SolarPACES*.